The Latitudinal Dependence of Atmospheric Jet Scales and Macroturbulent Energy Cascades

REI CHEMKE AND YOHAI KASPI

Department of Earth and Planetary Sciences, Weizmann Institute of Science, Rehovot, Israel

(Manuscript received 8 January 2015, in final form 8 April 2015)

ABSTRACT

The latitudinal width of atmospheric eddy-driven jets and scales of macroturbulence are examined latitude by latitude over a wide range of rotation rates using a high-resolution idealized GCM. It is found that for each latitude, through all rotation rates, the jet spacing scales with the Rhines scale. These simulations show the presence of a "supercriticality latitude" within the baroclinic zone, where poleward (equatorward) of this latitude, the Rhines scale is larger (smaller) than the Rossby deformation radius. Poleward of this latitude, a classic geostrophic turbulence picture appears with a $-5/3$ spectral slope of inverse cascade from the deformation radius up to the Rhines scale. A shallower slope than the -3 slope of enstrophy cascade is found from the deformation radius down to the viscosity scale as a result of the broad input of baroclinic eddy kinetic energy. At these latitudes, eddy–eddy interactions transfer barotropic eddy kinetic energy from the input scales of baroclinic eddy kinetic energy up to the jet scale and down to smaller scales. For the Earth case, this latitude is outside the baroclinic zone and therefore an inverse cascade does not appear. Equatorward of the supercriticality latitude, the $-5/3$ slope of inverse cascade vanishes, eddy–mean flow interactions play an important role in the balance, and the spectrum follows a -3 slope from the Rhines scale down to smaller scales, similar to what is observed on Earth. Moreover, the length scale of the energy-containing zonal wavenumber is equal to (larger than) the jet scale poleward (equatorward) of the supercriticality latitude.

1. Introduction

One of the most robust phenomena in geophysical fluid dynamics is the emergence of jets. These jets have a large impact on the dynamics of the atmosphere and ocean mostly through eddy–mean flow interactions and appear in both terrestrial and gas planets (e.g., Williams 1978; Panetta 1993; Schneider 2006). Because of their strong dependence on temperature gradients and heat fluxes in the atmosphere, these jets shape and feed off the zonal climatic bands on Earth. Furthermore, the wave patterns of these jets directly affect storm-track variability (Blackmon 1976; Blackmon et al. 1977). The main goal of this paper is to both develop a better understanding of the physical processes and properties controlling the jet spacing and width and to better understand how these vary as a function of latitude.

Corresponding author address: Rei Chemke, Department of Earth and Planetary Sciences, Weizmann Institute of Science, 234 Herzl St., Rehovot 7610001, Israel.
E-mail: rei.chemke@weizmann.ac.il

DOI: 10.1175/JAS-D-15-0007.1

In 2D turbulence, in the absence of vortex stretching, both energy and enstrophy are conserved resulting in an inverse energy cascade (Fjortoft 1953). In addition, the energy in the low-wavenumber regime is reduced by friction (e.g., Rivera and Wu 2000; Scott 2001; Smith et al. 2002; Danilov and Gurarie 2002; Grianik et al. 2004; Vallis 2006; Tsang and Young 2009). Kraichnan (1967) showed that in 2D turbulence the energy spectrum follows a $k^{-5/3}$ slope at small wavenumbers, where an inverse energy cascade occurs, while the enstrophy cascades to smaller scales, with an energy spectrum following a k^{-3} slope down to scales where dissipation by viscosity starts to play an important role (Lilly 1969; Scott 2001; Vallis 2006). While viscosity does not affect the absence of an inverse energy cascade in 2D turbulence, it does affect its time scale (Scott 2001).

Charney (1971) suggested that geostrophic turbulence in the atmosphere resembles 2D turbulence owing to conservation of pseudopotential vorticity, even though in the atmosphere vortex stretching plays a major role. Many observations verified that in Earth's atmosphere the energy spectra indeed behaves as in 2D turbulence with an energy spectrum following k^{-3}, but no inverse

cascade behavior at large scales (energy spectrum with a $k^{-5/3}$ power law) has been documented (e.g., Baer 1972; Boer and Shepherd 1983; Nastrom and Gage 1985; Koshyk and Hamilton 2001; Tung and Oralndo 2003). Moreover, Boer and Shepherd (1983) showed based on observations that while the higher-wavenumber regime corresponds to a power-law behavior, the low-wavenumber regime does not.

Rhines (1977) and Salmon (1978) showed that as the baroclinic energy cascades, while subtracting potential energy from the scale of the meridional temperature gradient down to the deformation radius (proportional to the most unstable wavelength according to linear theory; Eady 1949), it is converted to barotropic energy and inverse cascades to larger scales (e.g., Cai and Mak 1990). Several studies argued for barotropic (e.g., Berloff and Kamenkovich 2013b; Kobashi and Kawamura 2002; Scott and Wang 2005) and baroclinic (e.g., Scott and Wang 2005; Arbic et al. 2007) inverse energy cascades in the ocean.

Rhines (1975) showed that on a β plane, as in 2D turbulence, there is an inverse energy cascade from the stirring scale up to the Rhines scale, $L_\beta \propto \sqrt{U_{\rm rms}/\beta}$. At this scale, the regime of turbulent flow gradually changes to a Rossby wave regime. Vallis and Maltrud (1993) showed a similar scaling for the Rhines scale, but with a dependence on the energy cascade rate, by equating the anisotropic Rossby wave's frequency and the inverse of the eddy turnover time. Since Rossby waves transfer energy through resonant triad interactions (both in wave vectors and frequency), and because of the opposite dependence of frequency on wavenumber in both regimes, the upward energy cascade will be suppressed at the Rhines scale (Rhines 1975; Holloway and Hendershott 1977; Williams 1978; Rhines 1979; Danilov and Gurarie 2000; Galperin et al. 2006; Kaspi and Flierl 2007). However, the inverse energy cascade continues up to the largest scale in the system, $k_x = 0$, while in the k_y direction most of the energy remains close to the Rhines scale (Rhines 1975; Vallis and Maltrud 1993; Panetta 1993; Lee 2005; Scott and Polvani 2007; Thompson 2010; Srinivasan and Young 2012) and the formation of zonal jets occurs (e.g., Rhines 1977; Salmon 1978; Williams 1978; Vallis and Maltrud 1993; Rhines 1994).

Other studies found parameterizations other than the Rhines scale for the jet scale. Smith et al. (2002) showed that the arrest of the inverse energy cascade depends on the relative significance of the beta effect and the absorption of energy by friction. Moreover, surface drag was shown to affect the eddy scales and the energy ratio in the barotropic and baroclinic modes (Arbic et al. 2007). Sukoriansky et al. (2007) showed that Rossby waves and turbulence can coexist even in scales larger than the Rhines scale. Thus, the Rhines scale does not separate between the Rossby waves and turbulence regimes but plays different roles in different flow regimes; in unsteady flows, the Rhines scale is related to the inverse-cascading-energy front, while in a steady state the Rhines scale corresponds to scales of large-scale friction (zonostrophic regime; Galperin et al. 2006). Several studies used two-dimensional turbulence on the β plane and found an alternative scaling for the Rhines scale by taking friction into account and showing its proportionality with the meridional scale of the jets (e.g., Danilov and Gurarie 2002; Sukoriansky et al. 2007).

Schneider and Walker (2006) found that in an idealized GCM the meridional jet scale is similar to the Rossby radius, without inversely cascading to larger scales. O'Gorman and Schneider (2008b) showed that the meridional jet spacing approximately matches the scale of the energy-containing eddies, which does not vary much with latitude, and the Rhines scale as well. Farrell and Ioannou (2007) showed that under strong forcing the barotropic jet scale correlates with the Rhines scale through the Rayleigh–Kuo stability criterion and not through an inverse cascade argument. In their simulations for weak forcing the jet scale does not scale with the Rhines scale anymore but, rather, with the most unstable meridional wavenumber.

Stone (1978) developed an argument for baroclinic adjustment based on the supercriticality parameter [Eq. (3)] from the two-layer quasigeostrophic (QG) model (Phillips 1954). This argument states that the atmosphere is in a marginally critical state as a result of eddy fluxes that act to adjust the temperature gradients so the supercriticality parameter equals one. This was also verified using idealized GCM simulations over a wide range of parameters (Schneider and Walker 2006). One implication is that no inverse cascade occurs in an atmosphere that is in a marginally critical state. Indeed, as a result of the little separation between the scales of eddy generation and maximum eddy energy, barotropic inverse cascade was not observed on Earth (e.g., Boer and Shepherd 1983; Nastrom and Gage 1985; Shepherd 1987b), which implies that upscale energy transfer by nonlinear eddy–eddy interactions may play a minor role in the atmosphere (Panetta 1993; Schneider 2004; Schneider and Walker 2006; O'Gorman and Schneider 2007). As a result, the scale of the energy-containing eddies is similar to the deformation radius (Schneider and Walker 2006; O'Gorman and Schneider 2008b; Merlis and Schneider 2009).

On the other hand, Zurita-Gotor (2008) and Jansen and Ferrari (2012, 2013) showed that the

supercriticality parameter can vary above one, depending on the forcing that acts to change it. As the supercriticality parameter is much larger than one, nonlinear eddy–eddy interactions become important such that inverse cascade increases the scale of the energy-containing eddies (Zurita-Gotor and Vallis 2009; Jansen and Ferrari 2012; Chai and Vallis 2014). In those cases the Rossby deformation radius is not proportional to the scale of the energy-containing eddies anymore. However, as predicted by Rhines (1975), through all values of criticality the scale of the energy-containing eddies is proportional to the Rhines scale (Jansen and Ferrari 2012; Chai and Vallis 2014). By increasing the supercriticality parameter above one, Zurita-Gotor and Vallis (2009) showed the occurrence of the $k^{-5/3}$ spectrum. In addition, Jansen and Ferrari (2012, 2015) showed that regardless of supercriticality parameter the Rossby deformation radius is proportional to the scale where eddy available potential energy is converted to eddy kinetic energy (EKE).

Furthermore, Held and Larichev (1996) showed using a two-layer QG model that the supercriticality parameter also defines the ratio between the Rossby deformation radius and the Rhines scale. Hence, when the scale of the most unstable wave, which was predicted based on linear baroclinic theory (where potential energy is converted from the mean state to the eddies), is smaller than the scale that halts the inverse cascade, inverse cascade could occur and eddy–eddy interactions play an important role (Scott and Wang 2005). Moreover, it was shown using models (Theiss 2004; Sayanagi et al. 2008) and observations (Theiss 2006; Eden 2007) that geostrophic turbulence is isotropic (anisotropic) at latitudes where the Rhines scale is larger (smaller) than the Rossby deformation. Eden (2007) showed that the energy-containing scale was found to scale with the Rhines scale (Rossby deformation radius) when the flow was found to be anisotropic (isotropic). Okuno and Masuda (2003) and Smith (2004) showed that as the separation between the Rhines scale and Rossby deformation radius increases, the wave regimes and the Rhines effect are suppressed, and the flow is dominated by isotropic turbulence.

In this paper, because of these scales' dependence on both latitude and rotation rate, we do not integrate them over some baroclinic zone, as done in previous studies, but investigate the jet scales and energy cascades as function of latitude and rotation rate. Using simulations of latitudinally migrating eddy-driven jets (Chemke and Kaspi 2015) enables us to perform this analysis over a continuous range of latitudes at high rotation rates. The high rotation rates allow a better scale separation between the jet, Rhines and Rossby scales, and the radius of the planet. The latitudinal dependence of these scales is found to strongly imply the turbulent behavior of the flow. Section 2 describes the idealized GCM and analysis method. Scales for the jet spacing are presented in section 3, and their effect on the spectral slopes of the zonal barotropic EKE is presented in section 4. The zonal spectral budget of the barotropic EKE and the role of eddy–eddy interactions in affecting the zonal spectrum of the barotropic EKE are presented in sections 5 and 6, respectively. Sections 7 and 8 discuss the results and summarize them, respectively.

2. Model

We use an idealized aquaplanet moist global circulation model (GCM) based on the GFDL flexible modeling system (FMS). This is a spherical coordinate primitive equation model of an ideal gas atmosphere similar to Frierson et al. (2006) and O'Gorman and Schneider (2008a). The lower boundary of the model is an ocean slab with no topography. The model does not include any ocean dynamics (heat transport, etc.); thus, the surface temperature only changes as a result of heat transport between the ocean slab and the lower layer of the atmosphere via radiative energy, sensible heat, and latent heat fluxes. The parameterization of the surface fluxes (sensible heat, latent heat, and water vapor) and the boundary layer are based on the Monin–Obukhov similarity theory. The model contains a constant latitudinal distribution of solar radiation at the top of the atmosphere and a standard two-stream gray radiation scheme for longwave radiation with optical depths that are only a function of latitude and pressure (Goody 1964; Held 1982).

On Earth the eddy-driven jet is usually merged with the subtropical jet as the typical eddy scale is relatively large compared to the planet size. Thus, for studying the meridional scale of the eddy-driven jets we carry out a set of experiments where we systematically decrease the eddy length scale compared to the size of the planet by increasing the planetary rotation rate up to 16 times Earth's rotation rate Ω_e. The high rotation rates allow for separating the subtropical and eddy-driven jets and examining multijet planets with jets at all latitudes. All simulations have 30 vertical sigma layers at T170 horizontal resolution ($0.7° \times 0.7°$). Because of the poleward migration of the eddy-driven jets that was found in Chemke and Kaspi (2015), the results represent the time average of the last 500 days of 2500-day simulations. Choosing a shorter time average does not alter our results.

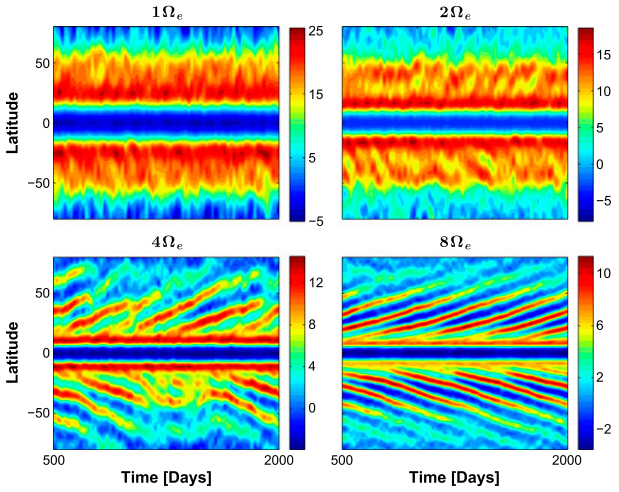

FIG. 1. Hovmöller diagrams of vertical and zonal mean zonal wind ($\mathrm{m\,s^{-1}}$) for simulations with 1, 2, 4, and $8\Omega_e$.

3. Jet spacing

In this work we use the simulations of Chemke and Kaspi (2015), where we have shown that at high rotation rates, the eddy-driven jets are clearly separated from the subtropical jets and, because of the sphericity of the planet, migrate poleward with time (Fig. 1). The constantly migrating eddy-driven jets at midlatitudes and high rotation rates allows for analyzing these jets with latitude across the entire baroclinic zone and mapping their spacing as a function of latitude and rotation rate (Fig. 2). The jet space is calculated as the meridional distance between two consecutive peaks of the zonal-mean zonal wind.[1] Because of the periodic migration of the eddy-driven jets (Fig. 1), we were able to accumulate statistics about the jets spacing at each latitude. The average of the jet spacing through all times at each latitude and rotation rate is plotted in Fig. 2. As simulations at higher rotation rates have more jets (Chemke and Kaspi 2015; Kaspi and Showman 2015), the space between the jets decreases with rotation rate. Thus, as in Schneider and Walker (2006), the total energy-containing wavenumber at $k = 0$ increases with rotation rate (Fig. 3). In addition, the jet spacing increases with latitude, as was pointed out by Huang and Robinson (1998) and Kidston and Vallis (2010).

As mentioned in the introduction, both the Rhines scale and the Rossby deformation radius have been related to the jet width. The fact that the jet spacing increases with latitude implies that the Rossby deformation radius likely does not solely set the jet spacing latitude by latitude. Based on Fig. 2, Fig. 4 shows the ratios between both the Rhines scale and the jet spacing, and the Rossby deformation radius and the jet spacing as a function of latitude for all simulated jets at all rotation rates presented in Fig. 2. The Rhines scale, following Rhines (1975), is calculated as

$$L_\beta = 2\pi\left[\frac{(\mathrm{EKE})^{1/2}}{\beta}\right]^{1/2}, \tag{1}$$

where $\mathrm{EKE} = u'^2 + v'^2$ is the vertically averaged eddy kinetic energy per unit mass, with the prime denoting deviations from the zonal mean, and β is the meridional derivative of the Coriolis parameter.[2]

The Rossby deformation radius is calculated as

$$L_D = 2\pi\frac{NH}{f}, \tag{2}$$

where f is the Coriolis parameter, H is the tropopause height calculated as the height where the static stability reaches a threshold value of $0.015\,\mathrm{s^{-1}}$, and $N^2 = (g/\theta)(\partial\theta/\partial z)$ is the vertically averaged static stability below the tropopause height [similar to Frierson et al. (2006)], where g is gravity and θ is the potential temperature. The Rossby deformation radius is found to be proportional to the deformation radius which is calculated as $f^{-1}\int N_p\,dp$ when applying the Liouville–Green or WKBJ approximation on the Sturm–Liouville eigenvalue problem for the vertical structure of the quasigeostrophic streamfunction (Gill 1982; Chelton et al. 1998), where $N_p = (g^2\rho/\theta)(\partial\theta/\partial p)$, p is pressure, and ρ is the density.

Three interesting properties can be seen in Fig. 4. First, the jet space seems to be well correlated with the Rhines scale, as suggested also by previous studies (e.g., Williams 1978; Panetta 1993; Vallis and Maltrud 1993; Thompson 2010), through all latitudes and rotation rates. Second, for each rotation rate there is a latitude where the Rhines scale is equal to the Rossby deformation radius (green line). Thus, poleward of these

[1] Calculating the jet width as the meridional distance between two consecutive minimum points of the zonal-mean zonal wind produces the same picture as in Fig. 2.

[2] We also explore other ways of calculating the Rhines scale, such as the barotropic Rhines scale using the barotropic EKE (deviation from zonal mean of the vertically averaged EKE; see appendix A) as done in previous studies (e.g., Haidvogel and Held 1980; Schneider and Walker 2006; Jansen and Ferrari 2012; Chai and Vallis 2014) and the Rhines scale based on the Rayleigh–Kuo stability criterion as suggested by Farrell and Ioannou (2007). Even though that the Rhines scale and the barotropic Rhines scale were found to be similar, none of these scales were found to have better scaling with the jet space and the scale of the energy-containing eddies than the scale in Eq. (1), as discussed further below.

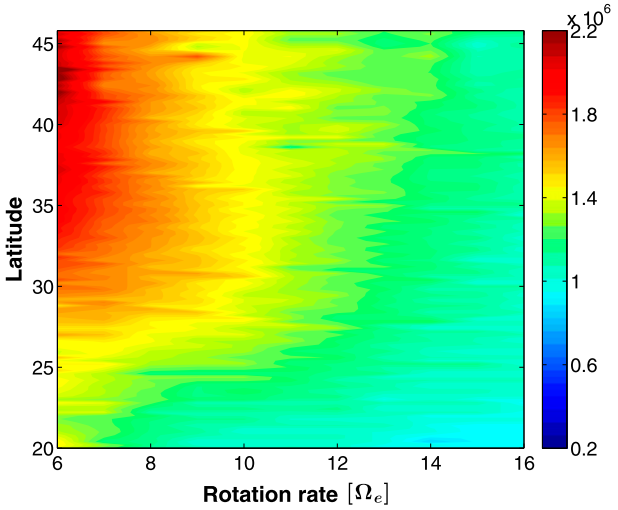

FIG. 2. Jet space (m) as function of latitude and rotation rate. The jet space is defined as the meridional length between two following maxima of the zonal wind. Only simulations with a continuous migration ($\Omega > 5\Omega_e$) were taken into account for the analysis of this figure.

latitudes the Rhines scale (blue dots) is larger than the Rossby deformation radius (red dots), and equatorward of these latitudes the Rossby deformation radius is larger than the Rhines scale (Theiss 2004). As mentioned in the introduction, Held and Larichev (1996) showed that the QG supercriticality follows the ratio of the Rhines scale and the Rossby deformation radius. The inset in Fig. 4 shows how this latitude separates the QG supercriticality (Phillips 1954; Held and Larichev 1996):

$$S_c = \frac{f^2 u_z}{\beta H N^2}, \tag{3}$$

where u_z is the vertical shear of the zonal wind, between values larger (black contours) and smaller (gray contours) than one for each rotation rate. Thus, in order to avoid confusion with the critical latitude related to Rossby waves, we assign this latitude as the "supercriticality latitude," since poleward of this latitude the QG supercriticality is larger than one (inset in Fig. 4) where inverse cascade could occur, and vice versa. The increase of the supercriticality with latitude is consistent with Jansen and Ferrari (2013) where an increase of $f\beta^{-1}$, while keeping the planet size constant, increases the supercriticality. The supercriticality latitude decreases with rotation rate, and this decrease becomes more moderate with rotation rate. This can be due to the opposite effects of the Coriolis parameter and the vertical shear of the zonal wind to increase and decrease, respectively, with rotation rate. If indeed the baroclinic energy is converted to barotropic energy at the Rossby deformation radius, as suggested by Salmon (1978), and the halting scale of the inverse cascade is the Rhines scale, as suggested by Rhines (1975), then this scale separation enables inverse energy cascade to occur only poleward of the supercriticality latitude. These points are discussed in sections 4 and 5 in more detail.

Third, poleward of this latitude where inverse cascade could occur, the Rhines scale is indeed more correlated with the jet space. This coincides with O'Gorman and Schneider (2008b), who showed that the eddy length scale was approximately the Rhines scale and the jet spacing as well. However, here the spacing between the jets increases with latitude, getting more moderate with rotation rate (Fig. 2). Equatorward of this latitude, where the Rossby deformation radius is larger than the Rhines scale, the Rhines scale still correlates, although not as well, with the jet space but better than the Rossby deformation radius.

The fact that the latitude where the Rossby deformation radius equals the Rhines scale increases as the rotation rate decreases (inset in Fig. 4) causes the width of the region where an inverse energy cascade can occur (where the Rhines scale is larger than the Rossby deformation radius) to decrease with decreasing rotation rate. On Earth, the Rhines scale and the Rossby deformation radius are nearly equal only at very high latitudes. This may explain why previous studies observed only the enstrophy cascade in the atmosphere with no inverse cascade (Baer 1972; Boer and Shepherd 1983; Lindborg 1999; Nastrom and Gage 1985; Koshyk and Hamilton 2001).

4. Zonal spectrum of the barotropic EKE

To understand the energy transport and jet scaling equatorward and poleward of the supercriticality latitude, we first examine the zonal spectrum of the barotropic EKE and then analyze its zonal spectral budget (section 5).

The meridional jet spacing (the Rhines scale; Fig. 4) does not necessarily play an important role in the energy transfers in the zonal direction. For example, Vallis and Maltrud (1993) and Huang and Robinson (1998) showed the anisotropic nature of the Rhines scale. Nonetheless, as we show below, the Rhines and the jet scales have a crucial role in affecting the processes which transport energy to the jet scale at each latitude in the zonal direction. Moreover, Huang and Robinson (1998) show this anisotropic nature of the Rhines scale by observing the energy-containing wavenumber of the kinetic energy in a zonal and total wavenumber space. In our simulations, on the other hand, the energy-containing wavenumber has a relative isotropic behavior, as it is

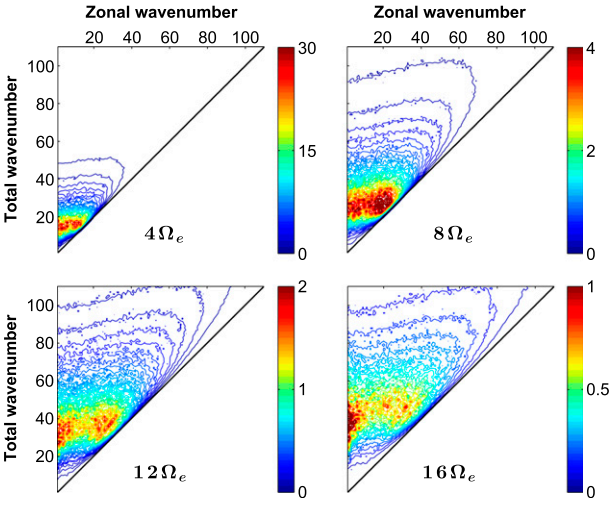

FIG. 3. The 2D spectrum, computed using spherical harmonics as basis functions (Boer and Shepherd 1983), of the barotropic EKE (10^{-2} m^2 s^{-2}) in the 4, 8, 12, and 16Ω_e simulations as a function of zonal and total wavenumbers.

almost parallel to the zonal wavenumber axis (Fig. 3). As in Boer and Shepherd (1983) and Shepherd (1987b), at large total wavenumbers and small zonal wavenumbers the turbulent regime of the barotropic flow becomes less isotropic. The fact that the contours of the barotropic EKE are spread along lines of constant total wavenumbers (Fig. 3) implies that if an inverse energy cascade occurs in the zonal direction (toward smaller zonal wavenumbers with higher energy), it is accompanied with an inverse energy cascade toward smaller total wavenumbers as well.

To demonstrate the latitudinal behavior of the barotropic EKE, we show its zonal spectrum for the 8Ω_e simulation at a latitude equatorward (Fig. 5a) and poleward (Fig. 5b) of the supercriticality latitude. We show only a sample of two latitudes, as these latitudes provide a representative picture of the barotropic EKE spectrum equatorward and poleward of the supercriticality latitude. We later show that these latitudes properly represent these two distinct regimes. At latitudes where the Rhines scale is smaller than the deformation radius (Fig. 5a), the barotropic EKE spectrum follows a k^{-3} slope of forward enstrophy cascade, as found on Earth, from the Rhines zonal wavenumber (blue asterisk; see appendix B) down to the viscosity scale.[3] This slope implies that nonlinear eddy–eddy interactions do not transport energy to larger scales. At latitudes where the Rhines scale is larger than the deformation radius (Fig. 5b), the spectral slope between the Rhines and Rossby zonal wavenumbers (red asterisk; see appendix B) indeed follows a $-5/3$ slope, as expected from the inverse cascade in 2D turbulence. Thus, eddy–eddy interactions transfer energy upscale from the deformation scale up to the jet scale. In addition, the spectral slope due to enstrophy cascade, from the Rossby zonal wavenumber to the viscosity scale, at latitudes poleward of the supercriticality latitude, is shallower than the expected -3 slope of enstrophy cascade. These two points are further explained in section 5. The energy plateau at large scales in Fig. 5b implies that the energy reaches the zero zonal wavenumber (the jet) as in Vallis and Maltrud (1993) by following the same contour of energy at the Rhines scale in their dumbbell figures. This can also be seen in Fig. 3 by following the energy-containing wavenumber contours, which separate two regimes at lower and higher wavenumbers with lower barotropic EKE. Alternatively, the maintenance of the jets can be by eddy–mean flow interactions (e.g., Shepherd 1987b; Panetta 1993; Huang and Robinson 1998; Robinson 2006; Farrell and Ioannou 2007), which we discuss in the next sections.

To see how robust this picture is, we calculate the above three slopes and plot the power of each slope as a function of rotation rate and latitude (Fig. 6). Each slope is calculated by fitting a linear trend to the log of the barotropic EKE over its specific wavenumber range. The red line shows the supercriticality latitude for each rotation rate. This line clearly separates between latitudes where the spectral slope is close to -3 between the Rhines zonal wavenumber and the viscosity scale (equatorward of the supercriticality latitude) and latitudes where the spectral slope is close to $-5/3$ between the Rhines and the Rossby zonal wavenumbers (poleward of the supercriticality latitude) for each rotation rate. The black contours show the spectral slopes between the Rossby zonal wavenumber down to the viscosity scale only for latitudes poleward of the supercriticality latitude. Through all latitudes and rotation rates, this slope is shallower than the -3 slope of enstrophy cascade. As we show later, this is because the conversion of baroclinic to barotropic EKE is spread through a wide range of scales (Larichev and Held 1995). For Earth parameters, this supercriticality latitude is poleward of the baroclinic region, which causes the atmosphere to show at each latitude inside the baroclinic region a spectral slope of -3, with no hint for inverse cascade (Fig. 6), which is consistent with Earth observations (e.g., Baer 1972; Boer and Shepherd 1983; Lindborg 1999; Nastrom and Gage 1985; Koshyk and

[3] We assign the viscosity scale at $k = 100$, where the zonal spectrum of the barotropic kinetic energy becomes extremely sharp. Despite the apparent arbitrariness of this choice, through all of the simulations this scale is always found to occur at the upper edge of the regime were viscosity starts to play a major role.

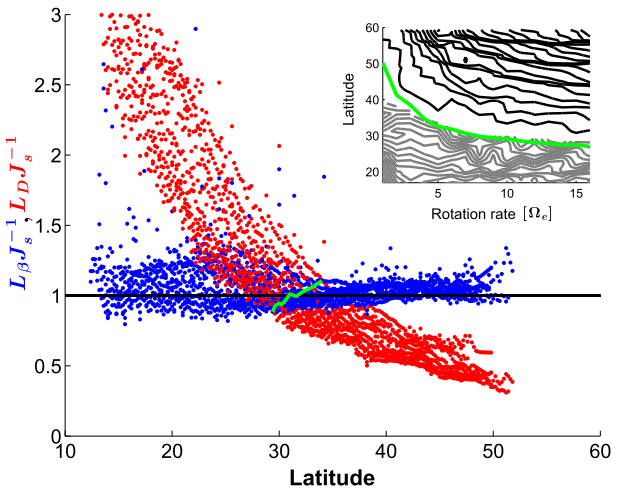

FIG. 4. The ratio between the Rhines scale and the jet spacing (blue) and between the Rossby deformation radius and the jet spacing (red) as a function of latitude for all simulations presented in Fig. 2. Each dot represents a single jet at a single latitude and rotation rate. The green line shows the supercriticality latitude where the Rhines scale equals the Rossby deformation radius. The inset shows the dependency of this latitude as a function of rotation rate. The black and gray contours show where the QG supercriticality $c_s S_c$ is larger and smaller than one, respectively. For demonstration purposes in this panel, $c_s = 1.5$ is an empirical constant chosen to best separate values larger and smaller than one around the supercriticality latitude. This choice does not affect the shape of the supercriticality with rotation rate (which follows the supercriticality latitude).

Hamilton 2001). This coincides with Frierson et al. (2006), who showed that on Earth through most of the baroclinic zone the deformation radius is larger than the Rhines scale.

At latitudes equatorward of the supercriticality latitude, the jet, Rhines, and Rossby zonal wavenumbers do not coincide with the energy-containing zonal wavenumber k_e calculated as in O'Gorman and Schneider (2008b) from the zonal spectrum of the barotropic meridional velocity (see appendix B). However, at latitudes poleward to the supercriticality latitude, the jet, Rhines, and the energy-containing zonal wavenumbers are almost indistinguishable, as in Jansen and Ferrari (2012), Chai and Vallis (2014), and in Schneider and Walker (2006) at simulations where their supercriticality was one. This could be robustly seen in Fig. 7; the jet scale is well correlated with the length scale of the energy-containing zonal wavenumber L_e (see appendix B) at latitudes poleward of the supercriticality latitude (blue dots) for all rotation rates. This coincides with Rhines's claim that the Rhines scale is the scale where the inverse energy cascade is being arrested (Rhines 1975). On the other hand, for latitudes equatorward of the supercriticality latitude (red dots), the jet scale is smaller than the length scale of the energy-containing zonal wavenumber. Schneider and Liu (2009) showed that in Jupiter simulations the Rhines scale and the length scale of the energy-containing zonal wavenumber coincide poleward to a certain latitude. However, different from our simulations, they found an opposite dependence of the spectral slope on latitude (Liu and Schneider 2015); in their simulations at equatorial latitudes, the zonal kinetic energy spectrum shows a $k^{-5/3}$ power law, but at midlatitudes the spectrum follows a k^{-3} slope.

Although the above picture strongly agrees with Rhines (1975) and Salmon (1978) at latitudes poleward of the supercriticality latitude where an inverse cascade occurs up to the jet scale, there are some features that require further explanation. First, it seems that even though the Rossby deformation radius coincides with the scale where inverse cascade begins (as can be seen by the $-5/3$ regime poleward of the supercriticality latitude), it fails to show the expected -3 slope of the enstrophy cascade (contours) but, rather, a shallower spectrum. Second, at high rotation rates ($>9\Omega_e$) the spectrum of the barotropic EKE below the supercriticality latitude is shallower than the k^{-3} that was observed at lower rotation rates (Fig. 6). And third, through most of the latitudes equatorward of the supercriticality latitude, the slopes get steeper than -3 as the latitude decreases (Fig. 6). These points are further discussed below.

5. Zonal spectral barotropic EKE budget

For interpretation of these results (Figs. 4 and 6), we proceed to analyze the different components in the barotropic EKE equation (see appendix A) similar to Larichev and Held (1995), only that here as a function of latitude. This allows us, first, to determine whether the Rossby deformation radius is indeed the scale where baroclinic energy is converted to barotropic energy. Second, it enables us to observe the behavior of eddy–eddy and eddy–mean flow interactions poleward and equatorward of the supercriticality latitude, and thus to better understand the processes of energy transport at latitudes where inverse cascade does and does not occur.

The results below are shown for the $8\Omega_e$ simulation as it captures the characteristics both above and below the supercriticality latitude. Hence, it is a representative picture of the behavior that occurs both at low and high rotation rates. Figure 8 shows four of the components of the barotropic EKE budget as function of latitude and zonal wavenumber. In each panel the Rhines zonal wavenumber (gray line), Rossby zonal wavenumber (black line), and the conversion zonal

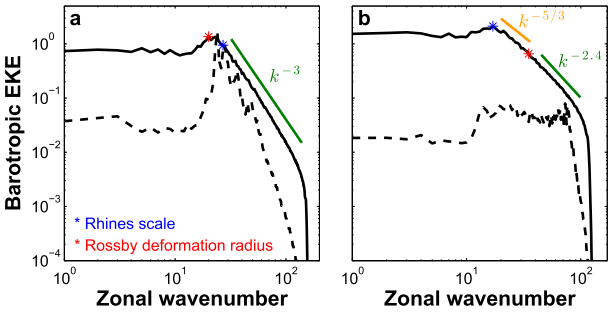

FIG. 5. The zonal spectrum of the barotropic EKE ($m^2 s^{-2}$) in the $8\Omega_e$ simulation as a function of zonal wavenumber with (solid black line) and without (dashed black line) eddy–eddy interactions for (a) a latitude where the Rhines scale is smaller than the Rossby deformation radius (25°) and (b) a latitude where the Rhines scale is larger than the Rossby deformation radius (45°). The spectrum of the barotropic EKE without eddy–eddy interactions is divided by 5 for a simpler comparison. The blue and red asterisks are the Rhines and Rossby zonal wavenumbers (see appendix B), respectively. In (a), the green line follows a k^{-3} slope. In (b), the orange and green lines follow a $k^{-5/3}$ and a $k^{-2.4}$ slope, respectively.

wavenumber (white line), which is calculated as the centroid [Eq. (B3)] of the conversion term [Eq. (A6)], are shown. In addition, the supercriticality latitude (blue line) and the conversion latitude, where the Rhines scale is equal to the conversion scale of baroclinic to barotropic EKE (red line), are plotted as well.

Most of the energy influx is from the baroclinic EKE (Fig. 8a). This influx is being transferred to larger (inverse cascade) and smaller scales (enstrophy cascade) by the eddy–eddy interactions (Fig. 8d). This transfer occurs mostly poleward of the supercriticality latitude and continues beyond the Rhines scale up to $k = 0$ (the energy plateau in Fig. 5 and following the energy-containing wavenumber contours in Fig. 3). At all latitudes above the supercriticality latitude, the Rhines scale captures well the upscale cascade by the eddy–eddy interactions (Fig. 8d). Thus, the arrest of the inverse cascade reaches larger scales at higher latitudes. This is opposite than the behavior documented by Scott and Wang (2005), who showed that the scale of the arrest of the inverse energy cascade in the ocean surface decreases with latitude. The eddy–mean flow interactions also remove energy around the supercriticality latitude; however, they add energy mostly equatorward of the supercriticality latitude at large scales (Fig. 8c). The conversion of barotropic EKE to eddy potential energy occurs at large scales while at intermediate scales barotropic eddy potential energy is converted to barotropic EKE. Note that the different terms presented in Fig. 8 contain not only the transport of barotropic EKE among different scales but also the lateral transport between different latitudes. This point is further discussed in section 7.

The Rossby deformation radius manages to separate accurately latitudes where the $-5/3$ slope of inverse cascade does and does not occur (Fig. 6); however, the corresponding Rossby zonal wavenumber does not coincide with the conversion zonal wavenumber (Fig. 8a). Alternatively, the supercriticality latitude could have been defined as the ratio between the Rhines scale and the conversion scale from baroclinic to barotropic EKE (Salmon 1978). However, this does not give three distinct regimes of the spectral slopes as shown by using the Rossby deformation radius (Fig. 6).[4] Thus, further investigation is needed for a better understanding of the role of the Rossby deformation radius in the energy cycle.

One reason that can explain the inability of the conversion zonal wavenumber or the Rossby zonal wavenumber to separate between the inverse energy cascade and the enstrophy cascade at each latitude, poleward of the supercriticality latitude (black contours in Fig. 6), is the wide range where baroclinic EKE is being converted to barotropic EKE (Figs. 8a and 9a). This was pointed out by Larichev and Held (1995), who showed that as a result of the broad conversion to the barotropic mode, the $-5/3$ slopes in the barotropic mode are steeper. One possibility is that this nonlocalization of energy conversion causes the slope, owing to the enstrophy cascade, to become shallower at latitudes poleward of the supercriticality latitude (Fig. 6). However, the $-5/3$ slope caused by the inverse energy cascade is less affected by this broadness (Fig. 6) since this broadness occurs mostly at wavenumbers larger than the Rossby and conversion zonal wavenumbers, as can be seen in Fig. 8a and from the long tail of the orange line in Fig. 9a.

As a result of the mismatch between the Rossby deformation radius and the conversion scale, there is a region between the supercriticality latitude and the conversion latitude (thus, between the red and blue lines) where the influx from the baroclinic EKE still occurs at scales smaller than the Rhines scale (Fig. 8a). Thus, at these latitudes the energy still needs to be transferred upscale to the jet scale. Indeed, eddy–eddy interactions are transferring energy upscale as well as downscale at these latitudes (Fig. 8d). However,

[4] The inability of the conversion latitude to produce such a sharp transition as occurs around the supercriticality latitude (Fig. 6) is also found for other conversion scales computed by different weighted-mean methods [e.g., Chai and Vallis (2014) used the inverse centroid of the conversion from eddy available potential energy to EKE, as in Schneider and Walker (2006)].

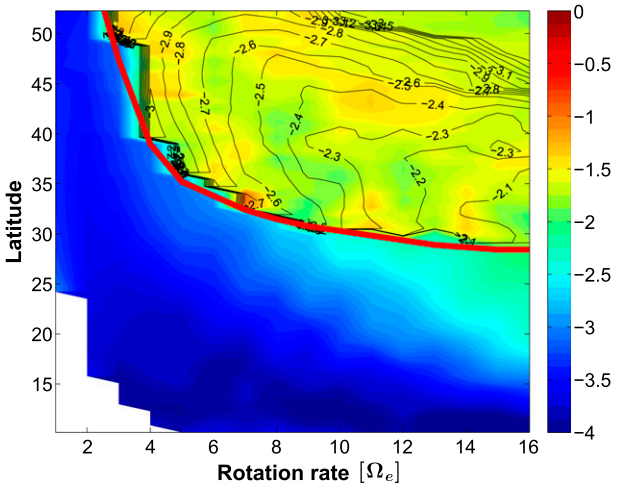

FIG. 6. The spectral slope as function of latitude and rotation rate. This is calculated as the power of the zonal wavenumber of a straight line fitted to the barotropic EKE spectrum for each latitude and rotation rate. The red line shows the latitude at each rotation rate where the Rhines scale equals the Rossby deformation radius. Below this line, the slope is fitted from the Rhines wavenumber down to $k = 100$. Above the red line, the slope is fitted between the Rhines wavenumber and the Rossby wavenumber. The contours show the spectral slope between the Rossby wavenumber and $k = 100$. The white area contains latitudes equatorward of the subtropical jet in each rotation rate.

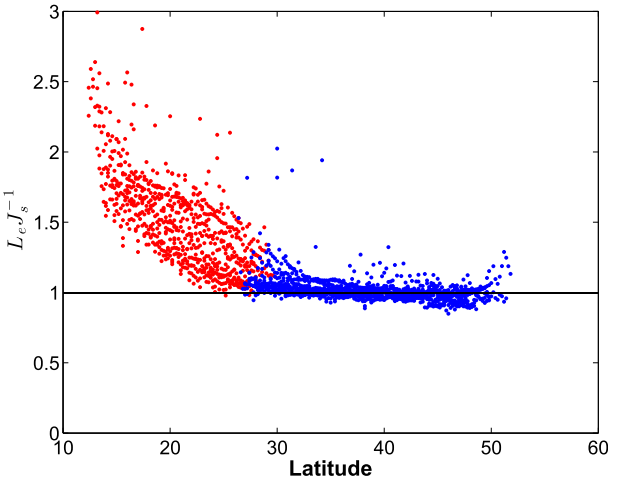

FIG. 7. The ratio of the length scale of the energy-containing zonal wavenumber, calculated from the zonal spectrum of the barotropic meridional velocity (see appendix B), and the jet space as a function of latitude for all rotation rates. The blue (red) dots represent latitudes poleward (equatorward) of the latitude where the Rhines scale is equal to the Rossby deformation radius.

equatorward of the supercriticality latitude, the slopes follow more the spectral slope of an enstrophy cascade k^{-3} (Figs. 5 and 6), rather than an inverse energy cascade. This could imply that an inverse cascade by eddy–eddy interactions equatorward of the supercriticality latitudes is weak and, thus, negligible in affecting the spectrum of the barotropic EKE to follow a $k^{-5/3}$ slope. Eddy–eddy interactions do seem to be weaker equatorward of the supercriticality latitude; however, their magnitude at large scales is similar to the magnitude of both the eddy–mean flow interactions and the conversion to barotropic eddy potential energy (Figs. 8b–d and 9b). In addition, unlike poleward latitudes where inverse cascade is observed, at these latitudes the jet scale is smaller than the length scale of the energy-containing zonal wavenumber (Fig. 7). We further discuss the role of eddy–eddy interactions poleward and equatorward of the supercriticality latitude in the next section.

We next focus on how the energy budget behaves equatorward of the conversion latitude (thus, equatorward of the red line), where the input to the barotropic EKE occurs at scales larger than the Rhines scale (Fig. 8). In terms of Vallis and Maltrud (1993)'s dumbbell figures, at these latitudes the influx of barotropic EKE occurs inside the dumbbell in the wave regime. The anisotropic nature of this regime disables us to infer any conclusions on the meridional jet spacing by studying the energy spectrum in the zonal direction. However, it is a unique regime and it is important to understand it in the zonal direction as well.

Figure 10 is similar to Fig. 8 but is only for latitudes equatorward of the conversion latitude. First, we can see that the magnitude of the different components in the barotropic EKE equation [Eq. (A1)] is an order of magnitude smaller than poleward of the conversion latitude. Second, at these latitudes the influx is mostly from barotropic eddy potential energy (Fig. 10b) rather than baroclinic EKE (Fig. 10a) as in the poleward latitudes (Fig. 8a). Moreover, only at these latitudes, the barotropic EKE is converted to baroclinic EKE at low latitudes and small wavenumbers (Fig. 8a). Different than the higher latitudes, here the eddy–mean flow interactions (Fig. 10c), which are stronger than the eddy–eddy interactions (Fig. 10d), transfer this influx from potential energy to higher latitudes. On the other hand, as the separation between the conversion wavenumber and the Rhines wavenumber grows (moving to lower latitudes) the eddy–eddy interactions remove the influx of barotropic eddy potential energy at large scales and transfer it down to the Rhines zonal wavenumber (Fig. 10d). At latitudes close to the conversion latitude, we can see the remnants of the influx from the baroclinic EKE and the outflux by both the eddy–eddy and eddy–mean flow interactions, in addition to the energy transfer to small scales by the eddy–eddy interactions.

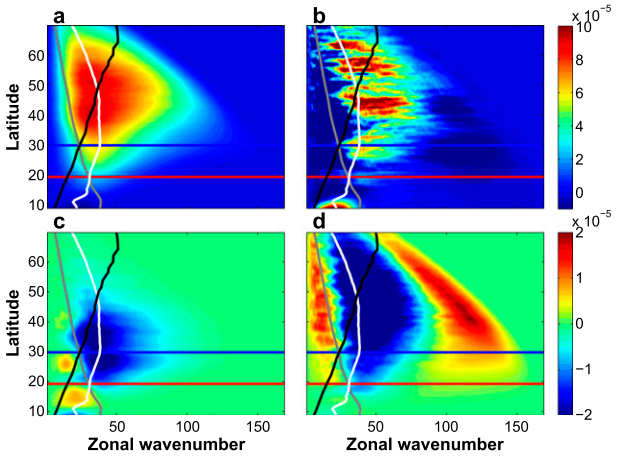

FIG. 8. Components of the barotropic EKE equation ($m^2 s^{-3}$; see appendix A) in the $8\Omega_e$ run as a function of latitude and zonal wavenumber: (a) conversion of baroclinic EKE, (b) conversion of barotropic eddy potential energy multiplied by 5, (c) eddy–mean flow interactions, and (d) eddy–eddy interactions. The gray, black, and white lines are the Rhines, Rossby, and the conversion zonal wavenumbers, respectively. The blue and red lines are the supercriticality and conversion latitudes, respectively. Each component is multiplied by the wavenumber and smoothed with a 20-point running mean.

6. The role of eddy–eddy interactions

To further analyze whether the eddy–eddy interactions are important poleward and equatorward of the supercriticality latitude, we remove the eddy–eddy interactions from the momentum and temperature equations as in O'Gorman and Schneider (2007). As a result, in these simulations only, the eddy–mean flow interactions can control the shape of the energy spectrum. The dashed black lines in Fig. 5 show the spectrum of the barotropic EKE in the simulation where we removed the eddy–eddy interactions. Although Fig. 5 shows only the spectrum of the barotropic EKE from two different latitudes (poleward and equatorward of the supercriticality latitude), their properties are found to be robust through all latitudes in this simulation. Similar to O'Gorman and Schneider (2007) and Chai and Vallis (2014), the barotropic EKE at intermediate scales, in the simulation with eddy–eddy interactions, is smaller than in the simulation where these interactions are absent (Fig. 5a). O'Gorman and Schneider (2007) suggested that the presence of eddy–eddy interactions reduces the competence to convert energy to barotropic energy and thus reduces the total barotropic kinetic energy. In addition, the removal of eddy–eddy interactions causes the spectrum to be less smooth (Fig. 5), likely as a result of the lack of energy transfer between different scales by these interactions (O'Gorman and Schneider 2007).

The spectrum of the barotropic EKE at latitudes poleward of the supercriticality latitude (Fig. 5b) does not follow a $k^{-5/3}$ slope anymore but, rather, a much shallower slope. As discussed in Shepherd (1987a), the tendency of the eddy–eddy interactions to spread the barotropic EKE along lines of constant total wavenumber (Fig. 3) vanishes in this simulation when they are absent (Fig. 11). Hence, similar to Berloff and Kamenkovich (2013a,b), the energy-containing wavenumber is more isolated in the spectral space (Figs. 5a and 11). This can also be observed in the simulation with eddy–eddy interactions, as the energy-containing zonal wavenumber (peaks of solid black lines in Fig. 5) is more (less) isolated at latitudes equatorward (poleward) of the supercriticality latitude, where eddy–eddy interactions are less (more) pronounced (note the logarithmic scale). These points strengthen the findings of sections 4 and 5 on the importance of eddy–eddy interactions, especially poleward of the supercriticality latitude, in transferring energy to larger scales.

On the other hand, equatorward of the supercriticality latitude the spectral slope at large scales qualitatively remains as in the simulation with the eddy–eddy interactions (Fig. 5a). Because of the lack of energy input by the eddy–mean flow interactions at small scales (as also occurs in the simulation with eddy–eddy interactions; Fig. 8c), the spectral slope becomes steeper at small scales. This could imply that as the eddy–eddy interactions weaken moving equatorward from the supercriticality latitude (Fig. 8d), the spectral slope should also become steeper (as can be seen in Fig. 6). Furthermore, equatorward of the conversion latitude, where eddy–eddy interactions are negligible (Fig. 10d), the tendency of the eddy–mean flow interactions to transfer energy to poleward latitudes along lines of constant zonal wavenumber (Fig. 10c) can also be seen in the simulation without eddy–eddy interactions where the barotropic EKE is more elongated along lines of constant zonal wavenumber (Fig. 11).

The importance of eddy–mean flow interactions, as seems to be the case equatorward of the supercriticality latitude (Figs. 8c and 9b), had been discussed in previous studies through shear-induced spectral transfer from the point of view of transient–stationary interactions (e.g., Shepherd 1987b; Huang and Robinson 1998). As in Huang and Robinson (1998), also here these interactions mostly involve eddies smaller than the Rhines scale (Fig. 8c), even though it correlates with the jet space (Fig. 4). Large-scale eddies also contribute to the spectral budget of the barotropic EKE (Fig. 8c). The lack of inverse cascade emphasizes the major role of eddy–mean flow interactions in maintaining the jets (Shepherd 1987b; Huang and Robinson 1998; Farrell

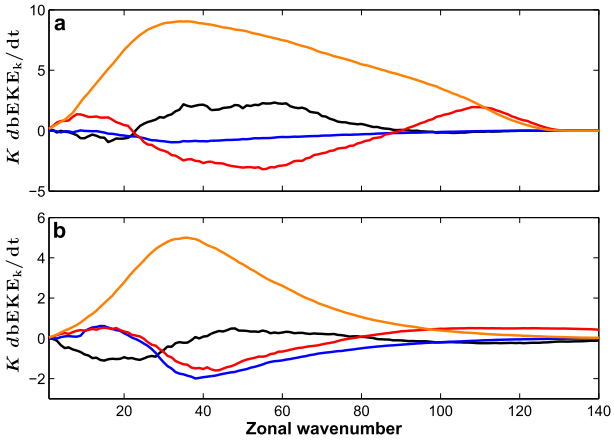

FIG. 9. Components of the barotropic EKE equation (10^{-5} m^2 s^{-3}; see appendix A) as a function of zonal wavenumber at latitudes (a) poleward of the supercriticality latitude (45°) and (b) equatorward of the supercriticality latitude (25°) in the $8\Omega_e$ run as in Fig. 8: conversion from baroclinic EKE to barotropic EKE (orange line), conversion from barotropic eddy potential energy to barotropic EKE (black line), transfer of barotropic EKE by eddy–eddy interactions (red line), and transfer from barotropic mean kinetic energy to barotropic EKE (blue line).

and Ioannou 2007) and adding energy at large scales. Therefore, other mechanisms other than an inverse energy cascade should explain the fact that the Rhines scale still coincides with the jet space equatorward of the supercriticality latitude. This point is beyond the scope of this paper and further discussed in the next section.

On Earth, the fact that the region between the supercriticality latitude and the subtropical jet covers the entire baroclinic zone (Fig. 6) may explain the fact that an inverse cascade is not observed in atmospheric observations (Baer 1972; Boer and Shepherd 1983; Lindborg 1999; Nastrom and Gage 1985; Koshyk and Hamilton 2001). Different than the higher-rotation-rate simulations, on Earth the relative large ratio between the eddy scale and the size of the planet causes only a small separation between the Rhines scale, the Rossby deformation radius, and the conversion scale at all latitudes. As a result, the minor role of eddy–eddy interactions in this regime at higher rotation rates (Fig. 8d) is not found in our Ω_e simulation.

7. Discussion

In this study, we show the importance of the Rossby deformation radius in affecting the spectrum of barotropic kinetic energy by distinguishing between latitudes where an inverse cascade does and does not occur (Fig. 6). However, different than the classic picture (e.g., Salmon 1978), this scale does not coincide with our measures of the conversion scale from baroclinic to barotropic EKE. Because of the mismatch between the Rossby deformation radius and the conversion scale, the influx from baroclinic to barotropic EKE at latitudes equatorward of the supercriticality latitude occurs at scales smaller than the Rhines scale. However, the spectrum of the barotropic EKE follows a k^{-3} slope. The lack of inverse cascade implies the minor role of eddy–eddy interactions in transferring energy upscale and the importance of eddy–mean flow interactions at these latitudes. In addition, since the length scale of the energy-containing zonal wavenumber at these latitudes is larger than the jet scale, other mechanisms besides an inverse energy cascade should explain the latitudinal coincident of the Rhines and jet scales. For example, Farrell and Ioannou (2007) showed that the barotropic jet scale could be determined by the Rayleigh–Kuo stability criterion (Kuo 1949); thus, with no inverse cascade, the jet scale should coincide with the Rhines scale, defined as $L_\beta = (U_{\max}/\beta)^{1/2}$, and could differ from the length scale of the energy-containing zonal wavenumber.

Several studies have shown that even by removing the nonlinear eddy–eddy interactions (quasi-linear models), the meridional structure of the jets remains similar to that in the full nonlinear simulations (e.g., O'Gorman and Schneider 2007; Constantinou et al. 2014; Srinivasan and Young 2012; Tobias and Marston 2013), thus implying that eddy–eddy interaction and inverse energy cascade might not be a prerequisite for jet formation. However, the different latitudinal spread of the ratio between the Rhines and jet scales poleward and equatorward of the supercriticality latitude (Fig. 4) implies that eddy–eddy interactions and inverse energy cascade do affect the meridional structure of the flow especially when it is highly nonlinear (e.g., poleward of the supercriticality latitude).

The spectrum of the barotropic EKE at latitudes equatorward of the supercriticality latitude at rotation rates higher than $9\Omega_e$ follows a shallower slope than the predicted -3 of enstrophy cascade as in 2D turbulence (Fig. 6). This is not due to not properly resolving the small-scale eddies, as simulations at T213 (0.56°) show the same behavior. One possibility is that as the rotation rate increases, the input of barotropic energy from both the barotropic eddy potential and baroclinic energies becomes broader at latitudes equatorward of the supercriticality latitude. As a result, the spectral slope can become shallower as occurs to the enstrophy cascade poleward of the supercriticality latitude. Alternatively, the decrease in accumulation of barotropic EKE by eddy–mean flow interactions at scales around the Rhines scale can also lead to a shallower slope.

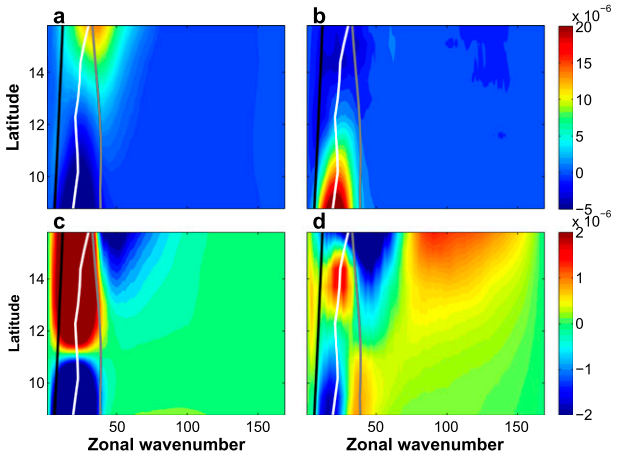

FIG. 10. Components of the barotropic EKE equation ($m^2 s^{-3}$; see appendix A) in the $8\Omega_e$ run as a function of latitude and zonal wavenumber, as in Fig. 8, only for latitudes where the Rhines scale is smaller than the conversion scale of baroclinic EKE: (a) conversion of baroclinic EKE, (b) conversion of barotropic eddy potential energy, (c) eddy–mean flow interaction, and (d) eddy–eddy interaction.

Our results show that the jet scale is proportional to the Rhines scale (Fig. 4). Assuming the jet and Rhines scales are equal, Lee (2005) suggested that the number of eddy-driven jets should be proportional to $\Omega^{0.5}$. However, in Chemke and Kaspi (2015), the number of eddy-driven jets follows $n_{\text{jet}} \propto \Omega^{0.81}$. These results may be different since in our simulations the baroclinic zone increases as the rotation rate increases (Fig. 6), while in Lee (2005) a constant width of baroclinic zone was taken into account.

The different terms in Fig. 8 [Eqs. (A3)–(A6)] contain not only the transport of barotropic EKE between different scales but also the lateral transport between different latitudes. However, by looking at Fig. 8d, it seems that most of the energy transfer is between different zonal scales and not between different latitudes. Theiss (2004) showed that the nonlinear interactions are responsible for the equatorward cascade of EKE, which we do not observe in our simulations. By summing the eddy–eddy and eddy–mean flow interactions over all zonal wavenumbers at each latitude, we observe the absence of the net lateral transport of barotropic EKE. The eddy–eddy interactions decrease by an order of magnitude once they are summed over all zonal wavenumbers with no coherent behavior of an equatorward cascade. Hence, these interactions transfer most of the barotropic EKE between different scales and do not seem to cascade energy toward the equator. The eddy–mean flow interactions, on the other hand, tend to remove the barotropic EKE through most latitudes.

Choi and Showman (2011) showed using the spectrum of cloud patterns imaged from the Cassini spacecraft that 2D turbulence inverse and enstrophy cascades could occur on Jupiter. Their transition scale between the $-5/3$ slope and -3 slope was found to be between approximately 1000 and 3000 km at a latitude of 45°. The planetary Rossby number of Jupiter, $U/\Omega R$, should be about 7 times smaller than that of Earth, as its radius is about 11 times larger than Earth's radius, its rotation rate is about 2.5 times faster, and its mean tropospheric winds are, on average, 4 times faster than those on Earth (Vasavada and Showman 2005). The Rossby deformation radius (which is found to be a potential transition scale in our simulations) at 45° in the $7\Omega_e$ simulation is indeed approximately 1000 km. On the other hand, other studies have shown that an inverse cascade does not necessarily occur on Jupiter (e.g., Schneider and Liu 2009). Theiss (2006) showed that by including the latitudinal dependency of the deformation radius in the dispersion relation of Rossby waves, the Rhines effect on Jupiter separates latitudes where coherent jets appear and where the flow is governed by vortices. This is consistent with findings by Theiss (2004), Sayanagi et al. (2008), and Scott and Polvani (2007); however, the fact that jets appear in our simulations even poleward of the supercriticality latitude (Figs. 1, 4, and 7) could imply that the shallow-atmosphere approximations in our PE model are not necessarily applicable to Jupiter's flow.

8. Conclusions

In this study we have used an idealized GCM at high rotation rates to allow a clear separation between the eddy-driven jet and the subtropical jet in the atmosphere. As the meridional jet spacing (latitudinal location) has an important effect on climate and weather systems, this separation enables us to scale the meridional spacing of the eddy-driven jets and study the macroturbulence behavior. Different from previous studies, the multiple-jet regime and their constant poleward migration at high rotation rates allow us to study the jet properties, macroturbulence, and energy cascades latitude by latitude and not just averaged over some baroclinic zone. Our main conclusions are as follows:

- The Rhines scale is able to predict the jet spacing latitude by latitude over a wide range of simulations with different rotation rates (Fig. 4).
- We show the presence of the supercriticality latitude: a latitude where the Rhines scale is equal to the Rossby deformation radius. We find that at latitudes poleward of the supercriticality latitude, where the Rhines scale is larger than the Rossby deformation radius, inverse energy cascade occurs from the Rossby

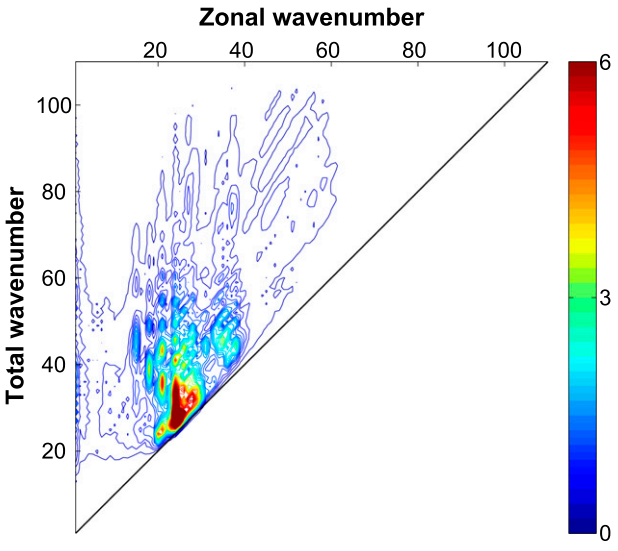

FIG. 11. The 2D spectrum of the barotropic EKE ($10^{-2}\,m^2\,s^{-2}$), as in Fig. 3, only for the $8\Omega_e$ simulation without eddy–eddy interactions, as a function of zonal and total wavenumbers.

deformation radius up to the Rhines scale with a spectral slope that follows a $k^{-5/3}$ slope as in two-dimensional turbulence (Fig. 6). In addition, at these latitudes, eddy–eddy interactions play a major role in cascading the barotropic EKE to larger and smaller scales (Fig. 8d). At these latitudes, the length scale of the energy-containing zonal wavenumber coincides with the jet scale (Fig. 7).

- At latitudes equatorward of the supercriticality latitude, where the Rhines scale is smaller than the Rossby deformation radius, there is a sharp transition to a regime where the spectral slope between the Rhines scale down to the viscosity scale follows a k^{-3} slope, similar to the enstrophy cascade in two-dimensional turbulence (Fig. 6).
- In our Earthlike simulations the supercriticality latitude is placed poleward of the baroclinic zone, causing it to produce only the k^{-3} slope of enstrophy cascade with no hint of inverse cascade (Fig. 6), as observed in Earth's atmosphere.
- Because of the nonlocal input of energy, mostly at small scales, from baroclinic to the barotropic EKE (Figs. 8a and 9a), the spectral slope of enstrophy cascade at latitudes poleward of the supercriticality latitude, from the Rossby deformation radius down to the viscosity scale, is shallower than the predicted k^{-3} slope (Fig. 6).
- Even though the Rossby deformation radius does not coincide with the scale where energy is being transferred from baroclinic to barotropic EKE (Fig. 8a), it still produces a sharp transition between latitudes where inverse cascade does and does not occur (Fig. 6).
- As a result of the previous point, at latitudes equatorward of the supercriticality latitude, the influx of baroclinic to barotropic EKE still occurs at scales smaller than the Rhines scale, even though the deformation radius is larger than the Rhines scale (Fig. 8a). Eddy–eddy interactions transfer energy upscale at these latitudes (Fig. 8d), although the spectral slope is similar to a k^{-3} of enstrophy cascade (Fig. 6). This implies that eddy–eddy interactions at these latitudes are too weak to affect the spectral slope. This, combined with the fact that the length scale of the energy-containing zonal wavenumber is larger than the jet scale at these latitudes (Fig. 7), emphasizes the minor role of the halting scale of the inverse energy cascade and the importance of eddy–mean flow interactions equatorward of the supercriticality latitude.
- By removing the eddy–eddy interactions from our model, we demonstrate the point above, and show that the spectral slope at these latitudes remains qualitatively the same at large scales because of eddy–mean flow interactions (Fig. 5). The importance of eddy–eddy interactions at latitudes poleward of the supercriticality latitude is also shown. In addition, at latitudes equatorward of the supercriticality latitude the eddy–eddy interactions transfer energy to larger and smaller scales (Fig. 8d), while the eddy–mean flow interactions add energy only at large wavenumbers (Fig. 8c). As a result, when eddy–eddy interactions are removed, the eddy–mean flow interactions alone produce at small scales a steeper spectral slope than the -3 of enstrophy cascade (Fig. 5). Thus, as we move to lower latitudes where the eddy–eddy interactions weaken (Fig. 8d), the spectral slope steepens as well (Fig. 6).
- At latitudes lower than the conversion latitude, where the Rhines scale is smaller than the conversion scale of baroclinic EKE and barotropic eddy potential energy to barotropic EKE, the eddy–mean flow interactions transfer the influx of energy from barotropic eddy potential energy to higher latitudes, while the eddy–eddy interactions spread it down to the Rhines scale. However, these transfers are much weaker than those at latitudes poleward of the conversion scale (Fig. 10).

Acknowledgments. We thank Janni Yuval for very fruitful discussions during the preparation of this manuscript. This research has been supported by an EU-FP7 Marie Curie Career Integration Grant (CIG-304202), the Israeli Science Foundation (Grants 1310/12 and 1859/12), and the Feinberg Graduate School at the Weizmann Institute of Science.

APPENDIX A

The Zonal Spectral Barotropic EKE Budget

We compute the zonal spectral barotropic EKE budget for each latitude. A similar latitudinal analysis was done by Saltsman (1957) only for the EKE. Unlike previous studies that investigated the spectral EKE equation using two-dimensional spectra (e.g., Lambert 1984; Koshyk and Hamilton 2001; Jansen and Ferrari 2012; Chai and Vallis 2014), here we compute the one-dimensional Fourier spectra of the barotropic EKE for each latitude. The zonal spectral barotropic EKE budget is computed as follows:

$$\frac{1}{2}\frac{\partial \mathrm{bEKE}}{\partial t} = \mathrm{EE} + \mathrm{EM} + P + \mathrm{CT} + F, \qquad \text{(A1)}$$

where

$$\mathrm{bEKE}_k = \langle |[u]'_k|^2 + |[v]'_k|^2 \rangle \qquad \text{(A2)}$$

is the zonal spectral barotropic EKE, angle brackets denote a time mean, square brackets denote a vertical average, and prime denotes the deviation from zonal mean (after taking the vertical average). The subscript k denotes the zonal spectral components with a zonal wavenumber k. The terms on the right-hand side of Eq. (A1) are as follows:

$$\mathrm{EE} = \left\langle \mathrm{Re}\left(-[u]^{\prime *}_k \left\{ ([\mathbf{u}]' \cdot \nabla [u]')_k - \left(\frac{[u]'[v]' \tan\theta}{a} \right)_k \right\} - [v]^{\prime *}_k \left\{ ([\mathbf{u}]' \cdot \nabla [v]')_k + \left(\frac{[u]'[u]' \tan\theta}{a} \right)_k \right\} \right) \right\rangle \qquad \text{(A3)}$$

contains the nonlinear eddy–eddy interactions,

$$\mathrm{EM} = \left\langle \mathrm{Re}\left(-[u]^{\prime *}_k \left\{ ([\overline{\mathbf{u}}] \cdot \nabla [u]')_k + ([\mathbf{u}]' \cdot \nabla [\overline{u}])_k - \left(\frac{[\overline{u}][v]' \tan\theta}{a} \right)_k - \left(\frac{[u]'[\overline{v}] \tan\theta}{a} \right)_k \right\} - [v]^{\prime *}_k \left\{ ([\overline{\mathbf{u}}] \cdot \nabla [v]')_k + ([\mathbf{u}]' \cdot \nabla [\overline{v}])_k + 2\left(\frac{[\overline{u}][u]' \tan\theta}{a} \right)_k \right\} \right) \right\rangle \qquad \text{(A4)}$$

contains the eddy–mean flow interactions,

$$P = \left\langle \mathrm{Re}\left(-[\mathbf{u}_H]^{\prime *}_k \left\{ (\nabla_H [\varphi]')_{\mathbf{k}} + \left(\frac{R[T]}{p_s} \nabla_H p_s \right)'_k \right\} \right) \right\rangle \qquad \text{(A5)}$$

contains the conversion of barotropic eddy potential energy to barotropic EKE,

$$\mathrm{CT} = \left\langle \mathrm{Re}\left\{ -[u]^{\prime *}_k \left([\mathbf{u}^+ \cdot \nabla u^+]'_k - \left[\frac{u^+ v^+ \tan\theta}{a} \right]'_k \right) - [v]^{\prime *}_k \left([\mathbf{u}^+ \cdot \nabla v^+]'_k + \left[\frac{u^+ u^+ \tan\theta}{a} \right]'_k \right) \right\} \right\rangle \qquad \text{(A6)}$$

contains the conversion of baroclinic EKE to barotropic EKE, and F contains the friction and diffusion terms, where $\mathbf{u}$ denotes the three-dimensional velocity vector, θ is latitude, the asterisk denotes a complex conjugate, the overbar denotes a zonal mean, the subscript H denotes a horizontal vector, p_s is the surface pressure, R is the specific gas constant, a is Earth's radius, and the plus-sign superscript denotes deviation from vertical average. The term of conversion of barotropic eddy potential energy [Eq. (A5)] is different than the usual term presented by Lorenz (1955), as here we do not integrate over the entire domain but, rather, keep our analysis as a function of latitude. Thus, as we do not add the continuity equation, we manage to keep the conversion term of barotropic eddy potential energy as simple as possible. In addition, as the model is in σ coordinates, the gradient of the surface pressure is added to the conversion of barotropic eddy potential energy term.

APPENDIX B

Eddy Scales

The energy-containing zonal wavenumber is calculated from the zonal spectrum of the barotropic eddy meridional velocity, similar to O'Gorman and Schneider (2008b):

$$k_e^2 = \frac{\sum_k |[v]'_k|^2}{\sum_k k^{-2} |[v]'_k|^2}. \qquad \text{(B1)}$$

As in O'Gorman and Schneider (2008b), we find that using the squared zonal wavenumber in the denominator

provides the energy-containing zonal wavenumber to be closest to the peak of the zonal spectrum of the barotropic eddy meridional velocity. The length scale of k_e is calculated for each latitude as follows:

$$L_e = \frac{2\pi a \cos(\theta)}{k_e}. \tag{B2}$$

The coincidence of the length scale of the energy-containing zonal wavenumber [Eq. (B2)] and the jet scale (Fig. 7) supports our choice of the power of k in Eq. (B1). The Rhines scale and Rossby deformation radius are converted to zonal wavenumbers using Eq. (B2). The conversion wavenumber of baroclinic to barotropic EKE is calculated as the centroid of Eq. (A6):

$$k_{\mathrm{CT}} = \frac{\sum_k k\mathrm{CT}}{\sum_k \mathrm{CT}}. \tag{B3}$$

This method produces wavenumber closest to the peak of the conversion of baroclinic to barotropic EKE (Fig. 8a).

REFERENCES

Arbic, B. K., G. R. Flierl, and R. B. Scott, 2007: Cascade inequalities for forced–dissipated geostrophic turbulence. *J. Phys. Oceanogr.*, **37**, 1470–1487, doi:10.1175/JPO3067.1.

Baer, F., 1972: An alternate scale representation of atmospheric energy spectra. *J. Atmos. Sci.*, **29**, 649–664, doi:10.1175/1520-0469(1972)029<0649:AASROA>2.0.CO;2.

Berloff, P., and I. Kamenkovich, 2013a: On spectral analysis of mesoscale eddies. Part I: Linear analysis. *J. Phys. Oceanogr.*, **43**, 2505–2527, doi:10.1175/JPO-D-12-0232.1.

——, and ——, 2013b: On spectral analysis of mesoscale eddies. Part II: Nonlinear analysis. *J. Phys. Oceanogr.*, **43**, 2528–2544, doi:10.1175/JPO-D-12-0233.1.

Blackmon, M. L., 1976: A climatological spectral study of the 500 mb geopotential height of the Northern Hemisphere. *J. Atmos. Sci.*, **33**, 1607–1623, doi:10.1175/1520-0469(1976)033<1607:ACSSOT>2.0.CO;2.

——, J. M. Wallace, N. Lau, and S. L. Mullen, 1977: An observational study of the Northern Hemisphere wintertime circulation. *J. Atmos. Sci.*, **34**, 1040–1053, doi:10.1175/1520-0469(1977)034<1040:AOSOTN>2.0.CO;2.

Boer, G. J., and T. G. Shepherd, 1983: Large-scale two-dimensional turbulence in the atmosphere. *J. Atmos. Sci.*, **40**, 164–184, doi:10.1175/1520-0469(1983)040<0164:LSTDTI>2.0.CO;2.

Cai, M., and M. Mak, 1990: Symbiotic relation between planetary and synoptic-scale waves. *J. Atmos. Sci.*, **47**, 2953–2968, doi:10.1175/1520-0469(1990)047<2953:SRBPAS>2.0.CO;2.

Chai, J., and G. K. Vallis, 2014: The role of criticality on the horizontal and vertical scales of extratropical eddies in a dry GCM. *J. Atmos. Sci.*, **71**, 2300–2318, doi:10.1175/JAS-D-13-0351.1.

Charney, J. G., 1971: Geostrophic turbulence. *J. Atmos. Sci.*, **28**, 1087–1095, doi:10.1175/1520-0469(1971)028<1087:GT>2.0.CO;2.

Chelton, D. B., R. A. Deszoeke, M. G. Schlax, E. Naggar, and N. Siwertz, 1998: Geographical variability of the first baroclinic Rossby radius of deformation. *J. Phys. Oceanogr.*, **28**, 433–460, doi:10.1175/1520-0485(1998)028<0433:GVOTFB>2.0.CO;2.

Chemke, R., and Y. Kaspi, 2015: Poleward migration of eddy driven jets. *J. Adv. Model. Earth Syst.*, doi:10.1002/2015MS000481, in press.

Choi, D. S., and A. P. Showman, 2011: Power spectral analysis of Jupiter's clouds and kinetic energy from Cassini. *Icarus*, **216**, 597–609, doi:10.1016/j.icarus.2011.10.001.

Constantinou, N. C., B. F. Farrell, and P. J. Ioannou, 2014: Emergence and equilibration of jets in beta-plane turbulence: Applications of stochastic structural stability theory. *J. Atmos. Sci.*, **71**, 1818–1842, doi:10.1175/JAS-D-13-076.1.

Danilov, S. D., and D. Gurarie, 2000: Quasi-two-dimensional turbulence. *Usp. Fiz. Nauk*, **170**, 921–968, doi:10.3367/UFNr.0170.200009a.0921.

——, and ——, 2002: Rhines scale and spectra of the beta plane turbulence with bottom drag. *Phys. Rev.*, **65E**, 067301, doi:10.1103/PhysRevE.65.067301.

Eady, E. T., 1949: Long waves and cyclonic waves. *Tellus*, **1**, 33–52, doi:10.1111/j.2153-3490.1949.tb01265.x.

Eden, C., 2007: Eddy length scales in the North Atlantic Ocean. *J. Geophys. Res.*, **112**, C06004, doi:10.1029/2006JC003901.

Farrell, B. F., and P. J. Ioannou, 2007: Structure and spacing of jets in barotropic turbulence. *J. Atmos. Sci.*, **64**, 3652–3665, doi:10.1175/JAS4016.1.

Fjortoft, R., 1953: On the changes in the spectral distribution of kinetic energy for twodimensional, nondivergent flow. *Tellus*, **5**, 225–230, doi:10.1111/j.2153-3490.1953.tb01051.x.

Frierson, D. M. W., I. M. Held, and P. Zurita-Gotor, 2006: A gray-radiation aquaplanet moist GCM. Part I: Static stability and eddy scale. *J. Atmos. Sci.*, **63**, 2548–2566, doi:10.1175/JAS3753.1.

Galperin, B., S. Sukoriansky, P. Read, Y. Yamazaki, and R. Wordsworth, 2006: Anisotropic turbulence and zonal jets in rotating flows with a beta effect. *Nonlinear Processes Geophys.*, **13**, 83–98, doi:10.5194/npg-13-83-2006.

Gill, A. E., 1982: *Atmosphere-Ocean Dynamics.* International Geophysics Series, Vol. 30, Academic Press, 662 pp.

Goody, R. M., 1964: *Atmospheric Radiation.* Clarendon Press, 436 pp.

Grianik, N., I. M. Held, K. S. Smith, and G. K. Vallis, 2004: The effects of quadratic drag on the inverse cascade of two-dimensional turbulence. *Phys. Fluids*, **16**, 73–78, doi:10.1063/1.1630054.

Haidvogel, D. B., and I. M. Held, 1980: Homogeneous quasi-geostrophic turbulence driven by a uniform temperature gradient. *J. Atmos. Sci.*, **37**, 2644–1660, doi:10.1175/1520-0469(1980)037<2644:HQGTDB>2.0.CO;2.

Held, I. M., 1982: On the height of the tropopause and the static stability of the troposphere. *J. Atmos. Sci.*, **39**, 412–417, doi:10.1175/1520-0469(1982)039<0412:OTHOTT>2.0.CO;2.

——, and V. D. Larichev, 1996: A scaling theory for horizontally homogeneous, baroclinically unstable flow on a beta plane. *J. Atmos. Sci.*, **53**, 946–952, doi:10.1175/1520-0469(1996)053<0946:ASTFHH>2.0.CO;2.

Holloway, G., and M. C. Hendershott, 1977: Stochastic closure for nonlinear Rossby waves. *J. Fluid Mech.*, **82**, 747–765, doi:10.1017/S0022112077000962.

Huang, H. P., and W. A. Robinson, 1998: Two-dimensional turbulence and persistent jets in a global barotropic model. *J. Atmos.*

Sci., **55**, 611–632, doi:10.1175/1520-0469(1998)055<0611:TDTAPZ>2.0.CO;2.

Jansen, M., and R. Ferrari, 2012: Macroturbulent equilibration in a thermally forced primitive equation system. *J. Atmos. Sci.*, **69**, 695–713, doi:10.1175/JAS-D-11-041.1.

——, and ——, 2013: Equilibration of an atmosphere by adiabatic eddy fluxes. *J. Atmos. Sci.*, **70**, 2948–2962, doi:10.1175/JAS-D-13-013.1.

——, and ——, 2015: Diagnosing the vertical structure of the eddy diffusivity in real and idealized atmospheres. *Quart. J. Roy. Meteor. Soc.*, **141**, 631–641, doi:10.1002/qj.2387.

Kaspi, Y., and G. R. Flierl, 2007: Formation of jets by baroclinic instability on gas planet atmospheres. *J. Atmos. Sci.*, **64**, 3177–3194, doi:10.1175/JAS4009.1.

——, and A. P. Showman, 2015: Three dimensional atmospheric dynamics of terrestial exoplanets over a wide range of orbital and atmospheric parameters. *Astrophys. J.*, **804**, 60, doi:10.1088/0004-637X/804/1/60.

Kidston, J., and G. K. Vallis, 2010: Relationship between eddy-driven jet latitude and width. *Geophys. Res. Lett.*, **37**, doi:10.1029/2010GL044849.

Kobashi, F., and H. Kawamura, 2002: Seasonal variation and instability nature of the North Pacific Subtropical Countercurrent and the Hawaiian Lee Countercurrent. *J. Geophys. Res.*, **107**, 3185, doi:10.1029/2001JC001225.

Koshyk, J. N., and K. Hamilton, 2001: The horizontal kinetic energy spectrum and spectral budget simulated by a high-resolution troposphere–stratosphere–mesosphere GCM. *J. Atmos. Sci.*, **58**, 329–348, doi:10.1175/1520-0469(2001)058<0329:THKESA>2.0.CO;2.

Kraichnan, R. H., 1967: Inertial ranges in two-dimensional turbulence. *Phys. Fluids*, **10**, 1417–1423, doi:10.1063/1.1762301.

Kuo, H. L., 1949: Dynamic instability of two-dimensional nondivergent flow in a barotropic atmosphere. *J. Meteor.*, **6**, 105–122, doi:10.1175/1520-0469(1949)006<0105:DIOTDN>2.0.CO;2.

Lambert, S. J., 1984: A global available potential energy-kinetic energy budget in terms of the two-dimensional wavenumber for the FGGE year. *Atmos.–Ocean*, **22**, 265–282, doi:10.1080/07055900.1984.9649199.

Larichev, V. D., and I. M. Held, 1995: Eddy amplitudes and fluxes in a homogeneous model of fully developed baroclinic instability. *J. Phys. Oceanogr.*, **25**, 2285–2297, doi:10.1175/1520-0485(1995)025<2285:EAAFIA>2.0.CO;2.

Lee, S., 2005: Baroclinic multiple zonal jets on the sphere. *J. Atmos. Sci.*, **62**, 2482–2498, doi:10.1175/JAS3481.1.

Lilly, D. K., 1969: Numerical simulation of two-dimensional turbulence. *Phys. Fluids*, **12**, 240–249, doi:10.1063/1.1692444.

Lindborg, E., 1999: Can the atmospheric kinetic energy spectrum be explained by two-dimensional turbulence? *J. Fluid Mech.*, **388**, 259–288, doi:10.1017/S0022112099004851.

Liu, J., and T. Schneider, 2015: Scaling of off-equatorial jets in giant planet atmospheres. *J. Atmos. Sci.*, **72**, 389–408, doi:10.1175/JAS-D-13-0391.1.

Lorenz, E. N., 1955: Available potential energy and the maintenance of the general circulation. *Tellus*, **7**, 157–167, doi:10.1111/j.2153-3490.1955.tb01148.x.

Merlis, T. M., and T. Schneider, 2009: Scales of linear baroclinic instability and macroturbulence in dry atmospheres. *J. Atmos. Sci.*, **66**, 1821–1833, doi:10.1175/2008JAS2884.1.

Nastrom, G. D., and K. A. Gage, 1985: A climatology of atmospheric wavenumber spectra of wind and temperature observed by commercial aircraft. *J. Atmos. Sci.*, **42**, 950–960, doi:10.1175/1520-0469(1985)042<0950:ACOAWS>2.0.CO;2.

O'Gorman, P. A., and T. Schneider, 2007: Recovery of atmospheric flow statistics in a general circulation model without nonlinear eddy-eddy interactions. *Geophys. Res. Lett.*, **34**, L22801, doi:10.1029/2007GL031779.

——, and ——, 2008a: The hydrological cycle over a wide range of climates simulated with an idealized GCM. *J. Climate*, **21**, 3815–3832, doi:10.1175/2007JCLI2065.1.

——, and ——, 2008b: Weather-layer dynamics of baroclinic eddies and multiple jets in an idealized general circulation model. *J. Atmos. Sci.*, **65**, 524–535, doi:10.1175/2007JAS2280.1.

Okuno, A., and A. Masuda, 2003: Effect of horizontal divergence on the geostrophic turbulence on a beta-plane: Suppression of the Rhines effect. *Phys. Fluids*, **15**, 56–65, doi:10.1063/1.1524188.

Panetta, R. L., 1993: Zonal jets in wide baroclinically unstable regions: Persistence and scale selection. *J. Atmos. Sci.*, **50**, 2073–2106, doi:10.1175/1520-0469(1993)050<2073:ZJIWBU>2.0.CO;2.

Phillips, N. A., 1954: Energy transformations and meridional circulations associated with simple baroclinic waves in a two level quasi-geostrophic model. *Tellus*, **6**, 273–286, doi:10.1111/j.2153-3490.1954.tb01123.x.

Rhines, P. B., 1975: Waves and turbulence on a beta plane. *J. Fluid Mech.*, **69**, 417–443, doi:10.1017/S0022112075001504.

——, 1977: The dynamics of unsteady currents. *Marine Modeling*, E. D. Goldberg et al., Eds., *The Sea: Ideas and Observations on Progress in the Study of the Seas*, Vol. 6, Wiley, 189–318.

——, 1979: Geostrophic turbulence. *Annu. Rev. Fluid Mech.*, **11**, 401–441, doi:10.1146/annurev.fl.11.010179.002153.

——, 1994: Jets. *Chaos*, **4**, 313–339, doi:10.1063/1.166011.

Rivera, M., and X. L. Wu, 2000: External dissipation in driven two-dimensional turbulence. *Phys. Rev. Lett.*, **85**, 976, doi:10.1103/PhysRevLett.85.976.

Robinson, W. A., 2006: On the self-maintenance of midlatitude jets. *J. Atmos. Sci.*, **63**, 2109–2122, doi:10.1175/JAS3732.1.

Salmon, R., 1978: Two-layer quasi-geostrophic turbulence in a simple special case. *Geophys. Astrophys. Fluid Dyn.*, **10**, 25–52, doi:10.1080/03091927808242628.

Saltsman, B., 1957: Equations governing the energetics of the larger scales of atmospheric turbulence in the domain of wave number. *J. Meteor.*, **14**, 513–523, doi:10.1175/1520-0469(1957)014<0513:EGTEOT>2.0.CO;2.

Sayanagi, K. M., A. P. Showman, and T. E. Dowling, 2008: The emergence of multiple robust zonal jets from freely evolving, three-dimensional stratified geostrophic turbulence with applications to Jupiter. *J. Atmos. Sci.*, **65**, 3947–3962, doi:10.1175/2008JAS2558.1.

Schneider, T., 2004: The tropopause and the thermal stratification in the extratropics of a dry atmosphere. *J. Atmos. Sci.*, **61**, 1317–1340, doi:10.1175/1520-0469(2004)061<1317:TTATTS>2.0.CO;2.

——, 2006: The general circulation of the atmosphere. *Annu. Rev. Earth Planet. Sci.*, **34**, 655–688, doi:10.1146/annurev.earth.34.031405.125144.

——, and C. C. Walker, 2006: Self-organization of atmospheric macroturbulence into critical states of weak nonlinear eddy–eddy interactions. *J. Atmos. Sci.*, **63**, 1569–1586, doi:10.1175/JAS3699.1.

——, and J. Liu, 2009: Formation of jets and equatorial superrotation on Jupiter. *J. Atmos. Sci.*, **66**, 579–601, doi:10.1175/2008JAS2798.1.

Scott, R. B., 2001: Evolution of energy and enstrophy containing scales in decaying, two-dimensional turbulence with friction. *Phys. Fluids*, **13**, 2739–2742, doi:10.1063/1.1388181.

——, and F. Wang, 2005: Direct evidence of an oceanic inverse kinetic energy cascade from satellite altimetry. *J. Phys. Oceanogr.*, **35**, 1650–1666, doi:10.1175/JPO2771.1.

——, and L. M. Polvani, 2007: Forced-dissipative shallow-water turbulence on the sphere and the atmospheric circulation of the giant planets. *J. Atmos. Sci.*, **64**, 3158–3176, doi:10.1175/JAS4003.1.

Shepherd, T. G., 1987a: Rossby waves and two-dimensional turbulence in a large-scale zonal jet. *J. Fluid Mech.*, **183**, 467–509, doi:10.1017/S0022112087002738.

——, 1987b: A spectral view of nonlinear fluxes and stationary-transient interaction in the atmosphere. *J. Atmos. Sci.*, **44**, 1166–1147, doi:10.1175/1520-0469(1987)044<1166:ASVONF>2.0.CO;2.

Smith, K. S., 2004: A local model for planetary atmospheres forced by small-scale convection. *J. Atmos. Sci.*, **61**, 1420–1433, doi:10.1175/1520-0469(2004)061<1420:ALMFPA>2.0.CO;2.

——, G. Boccaletti, C. C. Henning, I. Marinov, C. Y. Tam, and I. M. Held, 2002: Turbulent diffusion in the geostrophic inverse cascade. *J. Fluid Mech.*, **469**, 13–48, doi:10.1017/S0022112002001763.

Srinivasan, K., and W. R. Young, 2012: Zonostrophic instability. *J. Atmos. Sci.*, **69**, 1633–1656, doi:10.1175/JAS-D-11-0200.1.

Stone, P. H., 1978: Baroclinic adjustment. *J. Atmos. Sci.*, **35**, 561–571, doi:10.1175/1520-0469(1978)035<0561:BA>2.0.CO;2.

Sukoriansky, S., N. Dikovskaya, and B. Galperin, 2007: On the arrest of inverse energy cascade and the Rhines scale. *J. Atmos. Sci.*, **64**, 3312–3327, doi:10.1175/JAS4013.1.

Theiss, J., 2004: Equatorward energy cascade, critical latitude, and the predominance of cyclonic vortices in geostrophic turbulence. *J. Phys. Oceanogr.*, **34**, 1663–1678, doi:10.1175/1520-0485(2004)034<1663:EECCLA>2.0.CO;2.

——, 2006: A generalized Rhines effect and storms on Jupiter. *Geophys. Res. Lett.*, **33**, L08809, doi:10.1029/2005GL025379.

Thompson, A. F., 2010: Jet formation and evolution in baroclinic turbulence with simple topography. *J. Phys. Oceanogr.*, **40**, 257–278, doi:10.1175/2009JPO4218.1.

Tobias, S. M., and J. B. Marston, 2013: Direct statistical simulation of out-of-equilibrium jets. *Phys. Rev. Lett.*, **110**, 104502, doi:10.1103/PhysRevLett.110.104502.

Tsang, Y.-K., and W. R. Young, 2009: Forced-dissipative two-dimensional turbulence: A scaling regime controlled by drag. *Phys. Rev.*, **79**, 045308, doi:10.1103/PhysRevE.79.045308.

Tung, K. K., and W. W. Oralndo, 2003: The k^{-3} and $k^{-5/3}$ energy spectrum of atmospheric turbulence: Quasigeostrophic two-level model simulation. *J. Atmos. Sci.*, **60**, 824–835, doi:10.1175/1520-0469(2003)060<0824:TKAKES>2.0.CO;2.

Vallis, G. K., 2006: *Atmospheric and Oceanic Fluid Dynamics.* Cambridge University Press, 770 pp.

——, and M. E. Maltrud, 1993: Generation of mean flows and jets on a beta plane and over topography. *J. Phys. Oceanogr.*, **23**, 1346–1362, doi:10.1175/1520-0485(1993)023<1346:GOMFAJ>2.0.CO;2.

Vasavada, A. R., and A. P. Showman, 2005: Jovian atmospheric dynamics: An update after Galileo and Cassini. *Rep. Prog. Phys.*, **68**, 1935–1996, doi:10.1088/0034-4885/68/8/R06.

Williams, G. P., 1978: Planetary circulations: 1. Barotropic representation of the Jovian and terrestrial turbulence. *J. Atmos. Sci.*, **35**, 1399–1426, doi:10.1175/1520-0469(1978)035<1399:PCBROJ>2.0.CO;2.

Zurita-Gotor, P., 2008: The sensitivity of the isentropic slope in a primitive equation dry model. *J. Atmos. Sci.*, **65**, 43–65, doi:10.1175/2007JAS2284.1.

——, and G. K. Vallis, 2009: Equilibration of baroclinic turbulence in primitive equations and quasigeostrophic models. *J. Atmos. Sci.*, **66**, 837–863, doi:10.1175/2008JAS2848.1.